Supporting Information

Multi-Step Cation Substitution Facilitating the Exploration of Potential Infrared Nonlinear Optical Materials

Ya-Xiang Han[a, b], Chun-Li Hu[a], and Jiang-Gao Mao*[, a]

[a] *State Key Laboratory of Structural Chemistry, Fujian Institute of Research on the Structure of Matter, Chinese Academy of Sciences, Fuzhou, 350002, P. R. China.*

[b] *University of Chinese Academy of Sciences, Beijing 100039, P. R. China.*

Corresponding author: Jiang-Gao Mao, E-mail: mjg@fjirsm.ac.cn.

Section S1 Syntheses, Methods, and Reference

Reagent

   All the starting materials for synthesis of title compounds (purity higher than 99.9%) were purchased from Beijing Hawk Technology Co., Ltd. and has not been further purified.

Syntheses

   The Ag_2CdSiS_4, $BaAg_2SiS_4$ and $LaAgSiS_4$ single crystals were synthesized by high-temperature solid-state reactions described as below. In an argon gas-filled glovebox, the starting materials with a total weight of 0.3 grams were loaded into a clean graphite crucible, which was then placed into a quartz tube. The quartz tubes were sealed with hydrogen-oxygen flame under a high vacuum of 10^{-3} Pa. Subsequently, the quartz tubes were placed in a computer-controlled muffle furnace to allow the reactants to undergo a programmed temperature reaction.

   For the synthesis of Ag_2CdSiS_4, the Ag_2S, CdS, Si, and S powders with a molar ratio of 1:1:2:8 were heated to 300°C over 6 hours and held for 24 hours. Subsequently, the mixture was further heated to 850°C at a rate of 20°C/h. After holding at 850°C for 36 hours, the system was cooled to 750°C at a rate of 5°C/h and held for 36 hours, then further cooled to 650°C at 5°C/h and held for 24 hours. Finally, the tubes were cooled to 400°C at 5°C/h before turning off the furnace. Upon opening the crucibles, yellow block Ag_2CdSiS_4 crystals were obtained with a yield of approximately 70% with respect to Ag_2S reagent (Figure 2a).

   To synthesize $BaAg_2SiS_4$, the Ag_2S, BaS, and SiS_2 powders with a molar ratio of 1:1:2 were heated to 860°C with similar cooling process to Ag_2CdSiS_4. Dark yellow block $BaAg_2SiS_4$ crystals were obtained with a yield of approximately 80% with respect to Ag_2S reagent after the crucibles were opened (Figure 2b).

For the synthesis of LaAgSiS$_4$, the Ag$_2$S, La$_2$S$_3$, B, and S powders with molar ratio of 1: 0.75: 4: 6 and 0.2g SiO$_2$ were heated to 400°C within 8h and held for 24 h, then further heated to 900 °C at a rate of 25 °C/h. After holding for 48 h, the system was cooled to 800 °C at 5 °C/h and further cooled to 700 °C in 5 days. Finally, the tubes were cooled to 400 °C at 5 °C/h before turning the furnace off.[S1, S2] Yellow block LaAgSiS$_4$ crystals were found with a yield about 80% with respect to Ag$_2$S reagent after the crucibles opened (Figure 2c).

The microcrystalline powder used for tests was obtained by grinding small single crystals sonicated with deionized water and ethanol. The characterization details are described in supporting information.

Methods

Single Crystal X-ray Diffraction

Single-crystal X-ray diffraction data for Ag$_2$CdSiS$_4$, BaAg$_2$SiS$_4$ and LaAgSiS$_4$ were collected using an Agilent SuperNova dual-wavelength CCD diffractometer with Mo K$_\alpha$ radiation (λ = 0.71073Å). The CrysAlis Pro software package was utilized for data reduction. Numerical absorption corrections based on Gaussian integration over a multifaceted crystal model and empirical absorption corrections using spherical harmonics implemented in SCALE3 ABSPACK scaling algorithm were applied[S3]. The structures were determined by direct method and refined using full-matrix least-squares fitting on F^2 with SHELXL-2017[S4]. PLATON[S5] was used for checking symmetry elements and no higher was given. Crystal date was shown in table S1.

Powder X-ray Diffraction

Powder x-ray diffraction data were collected via Rigaku MiniFlex600 diffractometer. Scanning was performed with a scan step width of 0.02° using Cu Kα radiation (λ = 1.541886 Å) in the 2θ range of 10 – 70°.

Energy-Dispersive X-ray Spectroscopy

Elemental analyses were carried out using a field-emission scanning electron microscope (JSM6700F) outfitted with an Oxford INCA energy-dispersive X-ray spectroscope.

Infrared Spectrum

IR spectra were recorded on A Nicolet Magna 750 Fourier Transform Infrared spectrometer in the spectral range of 4000 to 400 cm^{-1}.

UV-Vis-NIR diffuse reflectance spectroscopy

The ultraviolet - visible - near-IR (UV-Vis-NIR) diffuse reflectance spectrum in the range of 200-2500nm was collected using a PerkinElmer Lambda 950 UV−vis−NIR spectrophotometer, with a barium sulfate powder plate as a 100% reflectance reference. Absorption data is converted from the reflection data by the Kubelka - Munk function $\alpha/S = (1 − R)^2/2R$ (α is the absorption coefficient, S the scattering coefficient, and R the reflectance. The band gap value is the abscissa of the intersection of the absorption edge extension line and the zero absorption.

Second-harmonic Generation measurements

SHG response measurements were performed using the Kurtz and Perry method with a 2.05 μm Q-switched Nd: YAG laser [S6]. Grind the crystals and sieve them into 6 particle sizes ranging from 45-53, 53-75, 75-105, 105-150, 150-210 and 210-300 μm, using microcrystalline $AgGaS_2$ with the same particle size range as a reference. The sample was placed on a glass microscope-covered slide, secured with a 1 mm thick silicone insole and a 5 mm diameter hole, and then covered with another glass slide.

They were then placed into small tight boxes and probed under the pulsed infrared beam of a Q-switched laser. The SHG signal was recorded on an oscilloscope connected to the detector. Standard IR NLO material of $AgGaS_2$ was used for all steps.

LIDT measurement

LIDT was measured using a 1 Hz 1064 nm Q-switch laser with $AgGaS_2$ as a reference. 150-210 μm particle size sample box was picked out for this test. For a point on the optical element (sample box), increasing pulse energy was raised from 1 mJ until the point is damaged.

Computational Method

Theoretical calculations were performed based on the single crystal structure data of Ag_2CdSiS_4, $BaAg_2SiS_4$ and $LaAgSiS_4$. The electronic structure and optical properties were analyzed by the plane wave pseudopotential method in the density functional theory (DFT) implemented in the total energy code CASTEP.[S7, S8] For the exchange and correlation functions, we chose Perdew-Burke-Ernzerhof (PBE) in the generalized Gradient Approximation (GGA).[S9] The interactions between the ionic cores and the electrons were described by the norm-conserving pseudopotential [S10]. The following valence-electron configurations were considered in the computation: Ag $4s^2 4p^6 4d^{10} 5s^1$, Cd $4d^{10} 5s^2$, Si $3s^2 3p^2$, S $3s^2 3p^4$ for Ag_2CdSiS_4; Ag $4s^2 4p^6 4d^{10} 5s^1$, Ba $5s^2 5p^6 6s^2$, Si $3s^2 3p^2$, S $3s^2 3p^4$ for $BaAg_2SiS_4$; Ag $4s^2 4p^6 4d^{10} 5s^1$, La $5d^1 6s^2$, Si $3s^2 3p^2$, S $3s^2 3p^4$ for $LaAgSiS_4$. The numbers of plane waves included in the basis sets were determined by cutoff energies of 765 eV. Monkhorst-Pack k-point samplings of 3×4×4, 4×4×3, 3×3×4 for Ag_2CdSiS_4, $BaAg_2SiS_4$ and $LaAgSiS_4$ respectively were used to perform numerical integration of the Brillouin zone. During the optical property calculations, approximately 156, 152 and 200 empty bands were involved to ensure the convergence of linear optical properties and SHG coefficients for Ag_2CdSiS_4, $BaAg_2SiS_4$ and $LaAgSiS_4$ respectively. The calculations of

second-order NLO properties were based on length-gauge formalism within the independent-particle approximation [S11]. We adopted Chen's static formula, which was derived by Rashkeev et al [S12]. and later improved by Chen's group [S13]. The static second-order NLO susceptibility can be expressed as

$$\chi^{\alpha\beta\gamma} = \chi^{\alpha\beta\gamma}(VE) + \chi^{\alpha\beta\gamma}(VH) + \chi^{\alpha\beta\gamma}(two\ bands)$$

where $\chi^{\alpha\beta\gamma}(VE)$ and $\chi^{\alpha\beta\gamma}(VH)$ give the contributions to $\chi^{\alpha\beta\gamma}$ from virtual-electron processes and virtual-hole processes, respectively, and $\chi^{\alpha\beta\gamma}(two\ bands)$ gives the contribution to $\chi^{\alpha\beta\gamma}$ from the two-band processes. The formulas for calculating $\chi^{\alpha\beta\gamma}(VE), \chi^{\alpha\beta\gamma}(VH), \chi^{\alpha\beta\gamma}(two\ bands)$ are given in ref S11.

References

(1) Lin S.; Mao J.; Guo G.; Huang J. *Journal of Alloys and Compounds* **1997**, *252*, L8–L11.

(2) Guo S.; Guo G.; Wang M.; Zou J.; Xu G.; Wang G.; Long X.; Huang J. *Inorg. Chem.* **2009**, *48*, 7059–7065.

(3) Blessing, R. H. *Acta Crystallogr. Sect. A: Found. Crystallogr.* **1995**, *51*, 33-38.

(4) Sheldrick, G. M. *Acta Crystallographica Section A: Foundation and Advances* **2015**, *71*, 3-8.

(5) Spek, A. L. *J. Appl. Crystallogr.* **2003**, *36*, 7-13.

(6) Kutz S. K.; Perry T. T. *J. Appl. Phys.* **1968**, *39*, 3798-3813.

(7) Milman, V.; Winkler, B.; White, J. A.; Pickard, C. J.; Payne, M. C.; Akhmatskaya, E. V.; Nobes, R. H. *Int. J. Quantum Chem.* **2000**, *77*, 895-910.

(8) Segall, M. D.; Lindan, P. J. D.; Probert, M. J.; Pickard, C. J.; Hasnip, P. J.; Clark, S. J.; Payne, M. C. *J. Phys.: Condens. Matter* **2002**, *14*, 2717-2744.

(9) Perdew, J. P.; Burke, K.; Ernzerhof, M. *Phys. Rev. Lett.* **1996**, *77*, 3865-3868.

(10) Lin, J. S.; Qteish, A.; Payne, M. C.; Heine, V. V. *Phys. Rev. B: Condens. Matter Mater. Phys.* **1993**, *47*, 4174-4180.

(11) Aversa, C.; Sipe, J. E. *Phys. Rev. B: Condens. Matter Mater. Phys.* **1995**, *52*, 14636-14645.

(12) Rashkeev, S. N.; Lambrecht, W. R. L.; Segall, B. *Phys. Rev. B: Condens. Matter Mater. Phys.* **1998**, *57*, 3905-3919.

(13) Lin, J.; Lee, M. H.; Liu, Z. P.; Chen, C. T.; Pickard, C. J. *Phys. Rev. B: Condens. Matter Mater. Phys.* **1999**, *60*, 13380-13389.

Table S1. Summary of Crystallographic data and structure refinements for Ag_2CdSiS_4, $BaAg_2SiS_4$ and $LaAgSiS_4$.

Formula	Ag_2CdSiS_4	$BaAg_2SiS_4$	$LaAgSiS_4$
formula weight	484.47	509.41	403.11
temperature (K)	294(2)	277(2)	279(2)
crystal system	Orthorhombic	Tetragonal	Orthorhombic
space group	*Pmn*2$_1$ (No.31)	*I*-42*m* (No.121)	*Ama*2 (No.40)
a (Å)	6.5238(12)	6.7561(3)	9.9125(5)
b (Å)	7.9574(15)	6.7561(3)	9.7832(5)
c (Å)	6.7820(14)	8.0095(6)	6.4529(3)
V (Å^3)	352.07(12)	365.59(4)	625.78(5)
Z	2	2	4
ρ_{calc} (g/cm^3)	4.570	4.628	4.279
μ (mm^{-1})	9.736	11.821	11.249
F(000)	440	456	728
λ (Mo Kα) (Å)		0.71073	
Rint	0.0659	0.0434	0.0477
Goodness-of-fit on F^2	1.082	1.104	1.052
R1, wR2 [I>2σ (I)][a]	0.0363, 0.0859	0.0185, 0.0409	0.0267, 0.0612
R1, wR2 (all data)	0.0424, 0.0901	0.0191, 0.0411	0.0271, 0.0616
flack parameter	-0.08(8)	0.02(2)	-0.04(2)

[a]$R_1 = \Sigma||F_o|-|F_c||/\Sigma|F_o|$; and $wR_2 = \{\Sigma[w(F_o^2-F_c^2)^2]/\Sigma[w(F_o^2)^2]\}^{1/2}$.

Table S2. Atomic coordinates ($\times 10^4$) and equivalent isotropic displacement parameters ($\text{Å}^2\times 10^3$) for for Ag_2CdSiS_4, $BaAg_2SiS_4$ and $LaAgSiS_4$. U_{eq} is defined as 1/3 of the trace of the orthogonalised UIJ tensor.

Compounds	Atom	x	y	z	U(eq)
Ag_2CdSiS_4	Ag(1)	7573(1)	1870(2)	1897(3)	29(1)
	Cd(1)	0	3505(3)	7059(4)	48(1)
	Si(1)	5000	3163(6)	7028(17)	13(1)
	S(1)	2784(5)	1725(5)	8072(8)	21(1)
	S(2)	5000	3113(9)	3767(10)	24(2)
	S(3)	10000	3902(8)	3151(9)	19(1)
$BaAg_2SiS_4$	Ba(1)	5000	5000	5000	13(1)
	Ag(1)	5000	10000	7500	34(1)
	Si(1)	10000	10000	5000	8(1)
	S(1)	8160(1)	8160(1)	6490(2)	13(1)
$LaAgSiS_4$	La(1)	5000	5000	3023(2)	10(1)
	Ag(1)	7500	6721(2)	8616(3)	62(1)
	Si(1)	7500	7850(5)	3181(10)	9(1)
	S(1)	7500	9363(4)	5537(7)	13(1)
	S(2)	7500	5978(5)	4917(7)	10(1)
	S(3)	5727(3)	7854(4)	1352(5)	14(1)

Table S3. Selected bond distances (Å) for for Ag_2CdSiS_4, $BaAg_2SiS_4$ and $LaAgSiS_4$.

Ag₂CdSiS₄					
Bond	**Length**	**Bond**	**Length**	**Bond**	**Length**
Cd(1)-S(1)	2.404(4)	Ag(1)-S(2)	2.325(5)	Si(1)-S(1)	1.975(7)
Cd(1)-S(1)#4	2.404(4)	Ag(1)-S(3)	2.418(4)	Si(1)-S(1)#3	1.975(7)
Cd(1)-S(3)#5	2.669(7)	Ag(1)-S(1)#1	2.607(5)	Si(1)-S(2)	2.212(17)
Cd(1)-S(2)#6	2.929(8)	Ag(1)-S(1)#2	2.973(5)	Si(1)-S(3)#7	2.456(8)
BaAg₂SiS₄					
Bond	**Length**	**Bond**	**Length**	**Bond**	**Length**
Ba(1)-S(1)#1	3.2465(13)	Ag(1)-S(1)	2.5997(5)	Si(1)-S(1)#12	2.1245(12)
Ba(1)-S(1)#2	3.2465(12)	Ag(1)-S(1)#10	2.5997(5)	Si(1)-S(1)#13	2.1245(12)
Ba(1)-S(1)#3	3.2465(12)	Ag(1)-S(1)#5	2.5997(5)	Si(1)-S(1)#14	2.1245(12)
Ba(1)-S(1)	3.2465(13)	Ag(1)-S(1)#11	2.5997(5)	Si(1)-S(1)	2.1245(12)
Ba(1)-S(1)#4	3.3161(13)				
Ba(1)-S(1)#5	3.3161(13)				
Ba(1)-S(1)#6	3.3161(13)				
Ba(1)-S(1)#7	3.3161(13)				
LaAgSiS₄					
Bond	**Length**	**Bond**	**Length**	**Bond**	**Length**
La(1)-S(2)#1	2.924(3)	Ag(1)-S(2)	2.495(5)	Si(1)-S(3)#8	2.117(5)
La(1)-S(2)	2.924(3)	Ag(1)-S(1)#5	2.619(5)	Si(1)-S(3)	2.117(5)
La(1)-S(1)#2	3.017(3)	Ag(1)-S(3)#6	2.727(4)	Si(1)-S(1)	2.122(7)
La(1)-S(1)#3	3.017(3)	Ag(1)-S(3)#7	2.727(4)	Si(1)-S(2)	2.147(7)
La(1)-S(3)#1	3.079(3)				
La(1)-S(3)	3.079(3)				
La(1)-S(3)#4	3.089(4)				
La(1)-S(3)#5	3.089(4)				

Symmetry transformations used to generate equivalent atoms:
Ag₂CdSiS₄:
#1 -x+1, y, z-1   #2 -x+2, y, z   #3 -x+1, y, z   #4 -x, y, z   #5 x-1, y, z   #6 -x+1/2, -y+1, z+1/2   #7 -x+3/2, -y+1, z+1/2
BaAg₂SiS₄:
#1 -x+1, -y+1, z   #2 -y+1, x, -z+1   #3 y, -x+1, -z+1   #4 x-1/2, y-1/2, z-1/2   #5 y-1/2, -x+3/2, -z+3/2
#6 -y+3/2, x-1/2, -z+3/2   #7 -x+3/2, -y+3/2, z-1/2   #8 -x+3/2, y-1/2, -z+3/2   #9 -x+1, y-1, -z+1   #10 -y+3/2, x+1/2, -z+3/2   #11 -x+1, -y+2, z   #12 -x+2, -y+2, z   #13 -y+2, x, -z+1
#14 y, -x+2, -z+1
LaAgSiS₄:
#1 -x+1, -y+1, z   #2 -x+1, -y+3/2, z-1/2   #3 x, y-1/2, z-1/2   #4 -x+1, -y+3/2, z+1/2   #5 x, y-1/2, z+1/2   #6 x-1/2, -y+1, z-1   #7 -x+3/2, y, z-1   #8 -x+3/2, y, z

Table S4. Local dipole moments of groups and units in Ag_2CdSiS_4, $BaAg_2SiS_4$ and $LaAgSiS_4$.

| Dipole moment (D = Debyes)		
Compounds / Polar unit	Ag_2CdSiS_4 (Z = 2)	$LaAgSiS_4$ (Z = 4)
SiS_4	5.689	5.191
AgS_4	3.936	4.275
CdS_4 / LaS_8	5.197	5.101
Net dipole moment (per unit)	18.028	54.060

Table S5. Measured LIDTs of for Ag_2CdSiS_4, $BaAg_2SiS_4$ and $LaAgSiS_4$.

Compounds	Spot area (cm^2)	Damage threshold (MW/cm^2)
Ag_2CdSiS_4	0.020	8.06
$BaAg_2SiS_4$	0.020	7.06
$LaAgSiS_4$	0.020	8.15
AGS	0.020	4.00

Figure S1. Morphologies of Ag_2CdSiS_4 (a), $BaAg_2SiS_4$ (b) and $LaAgSiS_4$ (c) crystals in $1mm^2$ reference dimension.
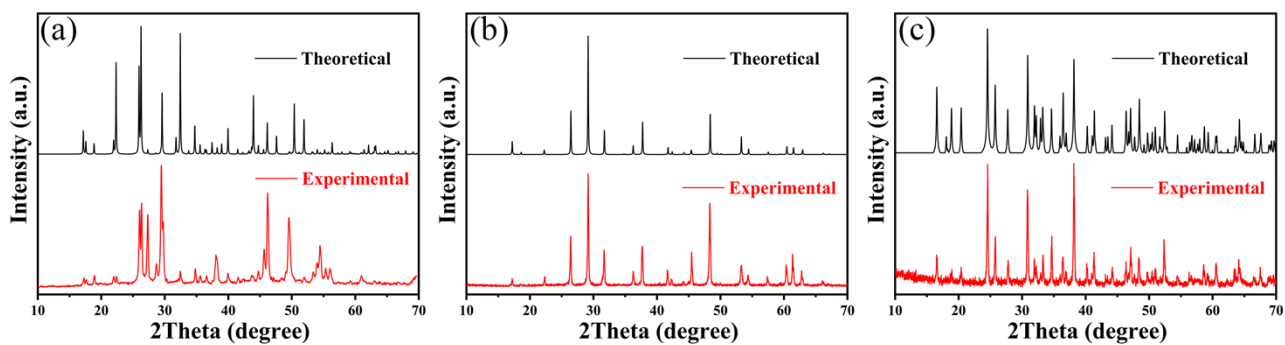
Figure S2. Simulated and measured powder X-ray diffraction patterns for Ag_2CdSiS_4, $BaAg_2SiS_4$ and $LaAgSiS_4$.
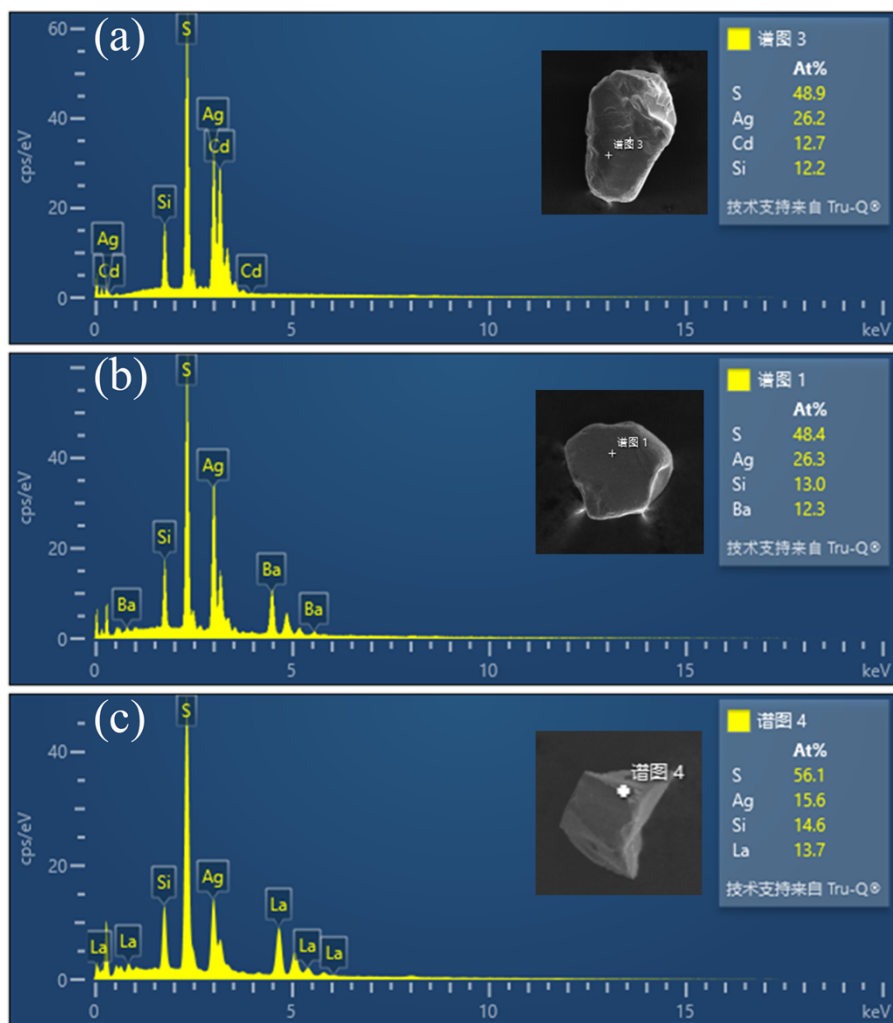
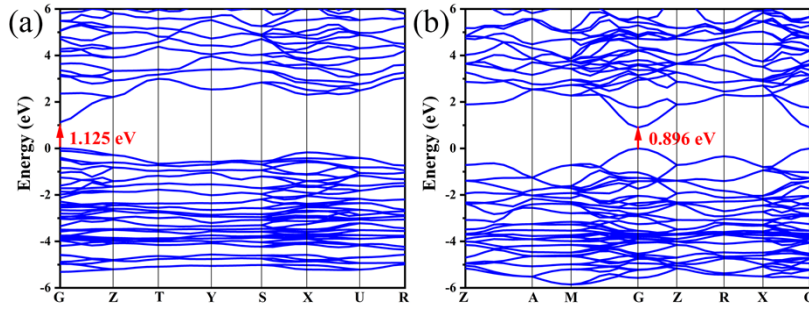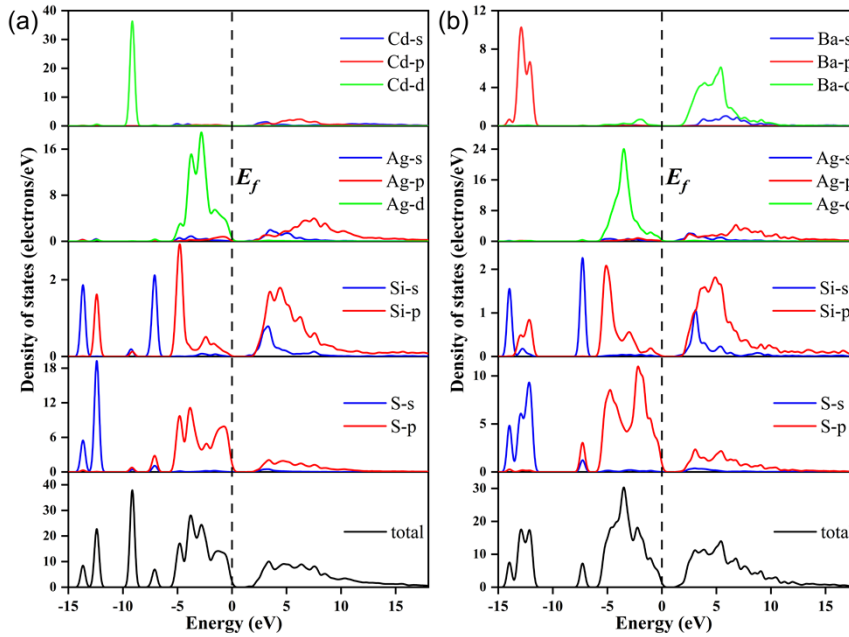**Figure S3.** EDS maps of Ag_2CdSiS_4 (a), $BaAg_2SiS_4$ (b) and $LaAgSiS_4$ (c).
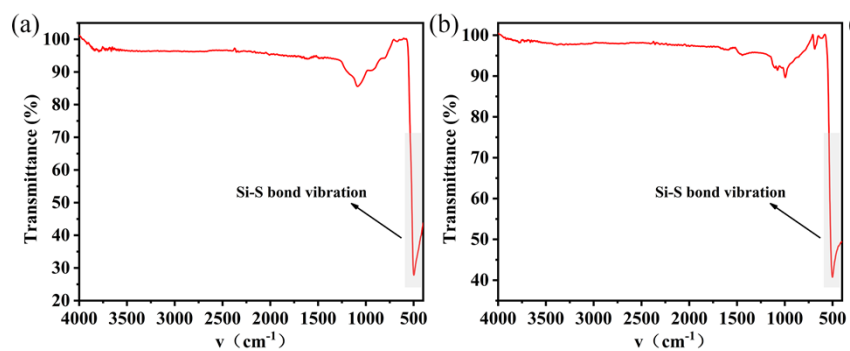
Figure S4. IR spectra for Ag_2CdSiS_4 (a) and $BaAg_2SiS_4$ (b).
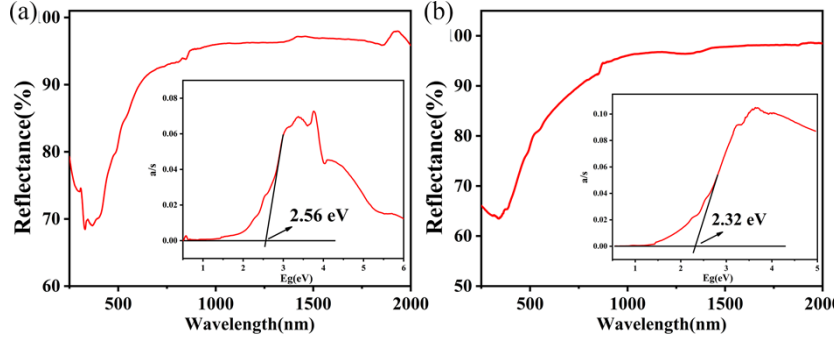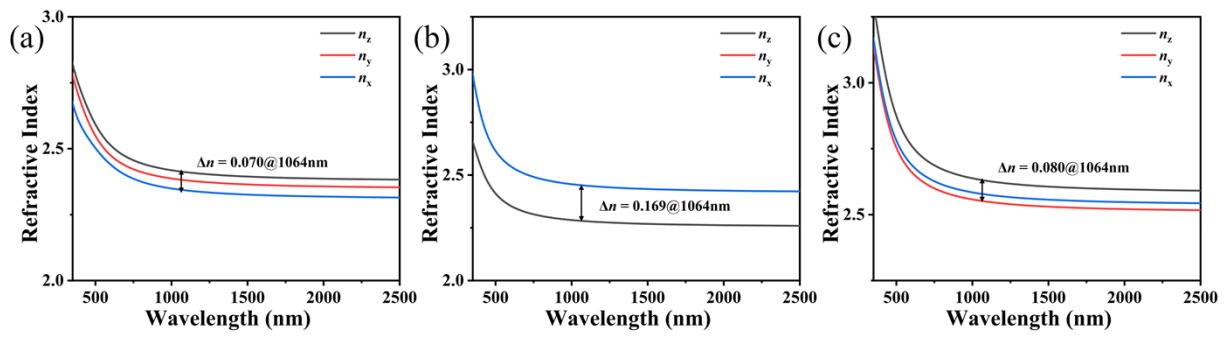
Figure S5. UV−vis−IR spectra for Ag_2CdSiS_4 (a) and $BaAg_2SiS_4$ (b).
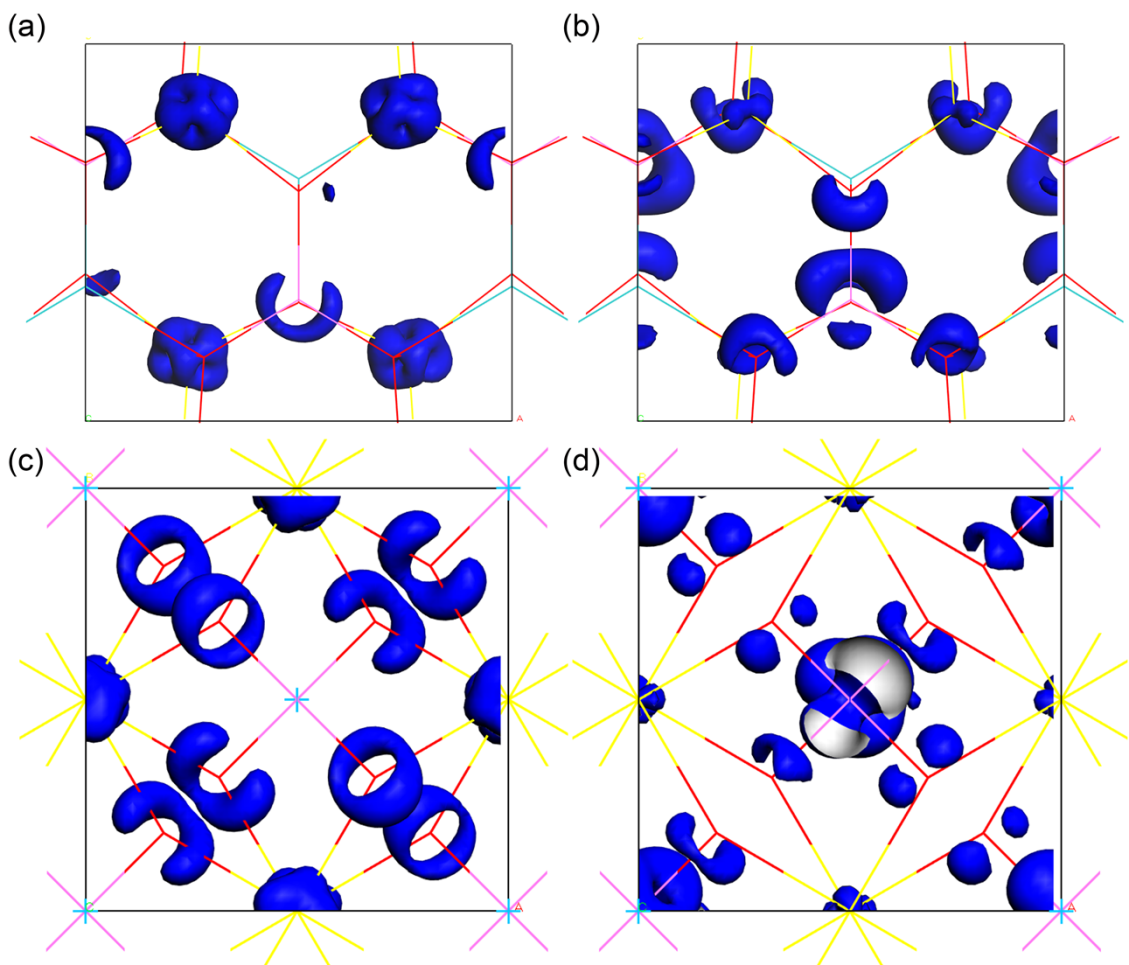

Figure S6. The calculated band structures for Ag_2CdSiS_4 (a) and $BaAg_2SiS_4$ (b).

Figure S7. The partial density of state for Ag_2CdSiS_4 (a) and $BaAg_2SiS_4$ (b).

Figure S8. The calculated refractive indices for Ag_2CdSiS_4 (a), $BaAg_2SiS_4$ (b) and $LaAgSiS_4$ (c).

Figure S9. SHG density plots for Ag_2CdSiS_4 [VB(a) and CB (b)] and $BaAg_2SiS_4$[VB (c) and CB (d)].